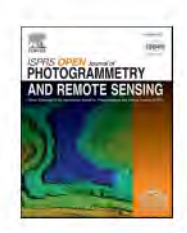
ELSEVIER

Contents lists available at ScienceDirect

ISPRS Open Journal of Photogrammetry and Remote Sensing

journal homepage: www.journals.elsevier.com/isprs-open-journal-of-photogrammetry-and-remotesensing





Estimation of lidar-based gridded DEM uncertainty with varying terrain roughness and point density

Luyen K. Bui a,b,*, Craig L. Glennie

- a Department of Civil and Environmental Engineering, University of Houston, Houston, TX, 77386, United States
- ^b Faculty of Geomatics and Land Administration, Hanoi University of Mining and Geology, Hanoi, Viet Nam

ARTICLEINFO

Keywords: LIDAR TIN Interpolation Uncertainty propagation Terrain roughness Point density

ABSTRACT

Light detection and ranging (lidar) scanning systems can be used to provide a point cloud with high quality and point density. Gridded digital elevation models (DEMs) interpolated from laser scanning point clouds are widely used due to their convenience, however, DEM uncertainty is rarely provided. This paper proposes an end-to-end workflow to quantify the uncertainty (i.e., standard deviation) of a gridded lidar-derived DEM. A benefit of the proposed approach is that it does not require independent validation data measured by alternative means. The input point cloud requires per point uncertainty which is derived from lidar system observational uncertainty. The propagated uncertainty caused by interpolation is then derived by the general law of propagation of variances (GLOPOV) with simultaneous consideration of both horizontal and vertical point cloud uncertainties. Finally, the interpolated uncertainty is then scaled by point density and a measure of terrain roughness to arrive at the final gridded DEM uncertainty. The proposed approach is tested with two lidar datasets measured in Waikoloa, Hawaii, and Sitka, Alaska. Triangulated irregular network (TIN) interpolation is chosen as the representative gridding approach. The results indicate estimated terrain roughness/point density scale factors ranging between 1 (in flat areas) and 7.6 (in high roughness areas), with a mean value of 2.3 for the Waikoloa dataset and between 1 and 9.2 with a mean value of 1.2 for the Sitka dataset. As a result, the final gridded DEM uncertainties are estimated between 0.059 m and 0.677 m with a mean value of 0.164 m for the Waikoloa dataset and between 0.059 m and 1.723 m with a mean value of 0.097 m for the Sitka dataset.

1. Introduction

Digital elevation models (DEMs) are representations of the Earth's surface, and are used for a wide range of applications including hydrology, geomorphology, and environmental modeling (Wechsler and Kroll, 2006). DEMs can be generated by various methods, such as laser scanning (Liu, 2008), Interferometric Synthetic Aperture Radar (InSAR) (Rabus et al., 2003), global navigation satellite system (GNSS) (Abd Aziz et al., 2009), photogrammetry (Ouédraogo et al., 2014), and total stations (Fuller et al., 2003). In all cases measurement errors influence the DEMs' quality, which can be assessed by comparison with an independent reference surface (Brasington et al., 2000, 2003). However, a reference surface is not always available and therefore an alternative approach is to use independently measured data or diagnostic surface visualization (Heritage et al., 2009). By using independently measured data, DEM accuracy can be represented by statistical quantities of the difference between the DEM and independent measurements at discrete

points, e.g., Root Mean Square Error (RMSE) (Aguilar et al., 2010; Su and Bork, 2006; Spaete et al., 2011; Wechsler and Kroll, 2006), or standard deviation (STD) (Carlisle, 2005; Wechsler and Kroll, 2006). Independent samples not used for DEM construction can be used for assessing interpolation errors rather than for absolute DEM accuracy. However, this requires measurements made by a method other than that used in DEM generation, e.g., GNSS, total station, or leveling. Moreover, these data should be of higher accuracy and do not normally have the same characteristics as those of the DEM in terms of spatial density and coverage.

Airborne laser scanning (ALS) is a method that has been widely applied as topographic measurements to generate DEMs. ALS has the advantages of high accuracy and density with no dependence on solar illumination (Glennie et al., 2013). Uncertainty of the light detection and ranging (lidar) point cloud can also be estimated without the requirement for high quality independent measurements, based on errors from GNSS-based positioning, Inertial Measurement Unit (IMU)

^{*} Corresponding author. Department of Civil and Envionmental Engineering, University of Houston, Houston, TX, 77386, United States. E-mail address: buikhacluyen@humg.edu.vn (L.K. Bui).

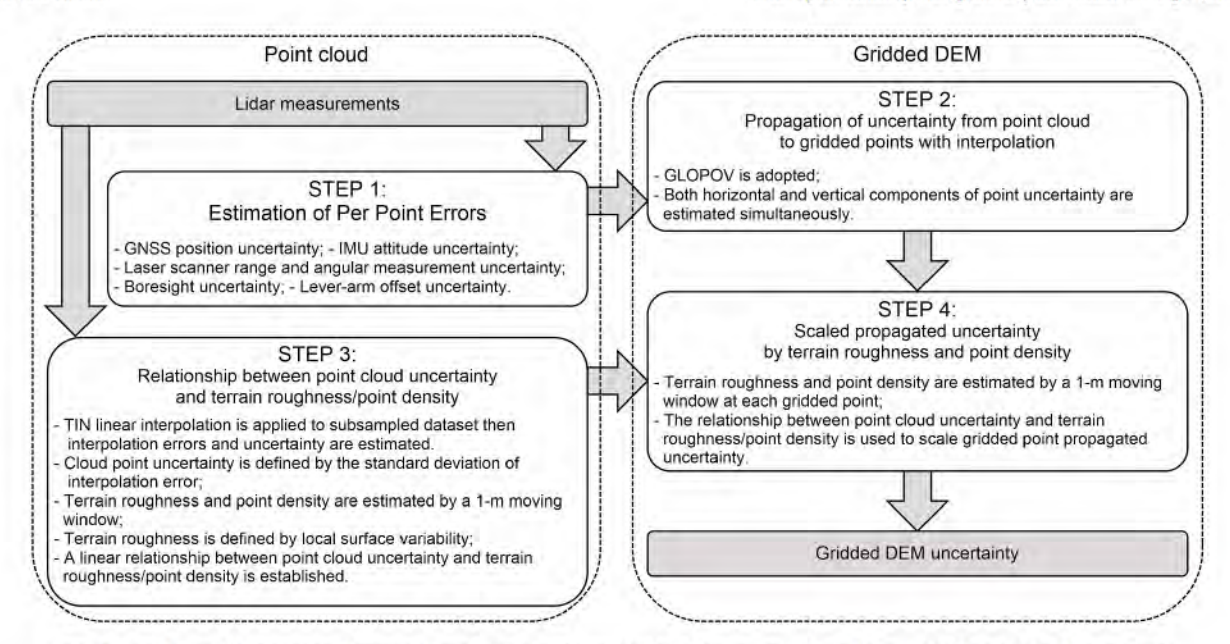


Fig. 1. Workflow of the proposed approach used to estimate gridded DEM uncertainty from lidar-derived point cloud uncertainty.

attitude, laser angular measurements, boresight angles, and lever-arm offsets (Glennie, 2007). Though a dense and irregular dense and irregular point cloud is one of the benefits of laser scanning, a gridded DEM is frequently utilized (Glennie et al., 2013), which is generated by interpolation by, e.g., nearest neighbor (Kidner, 2003), triangulated irregular network (TIN) (Fan et al., 2014), linear (Kyriakidis and Goodchild, 2006), high-order polynomials (Shi et al., 2005), inverse distance weighted (IDW) (Aguilar et al., 2010), and Kriging (Rees, 2000); among which, TIN is the most popular. Therefore, a gridded DEM's uncertainty is composed of 1) lidar point uncertainty, 2) uncertainty propagated through interpolation, and is influenced by 3) the density of the observations and 4) the roughness of the observed surface (Agüera-Vega et al., 2020; Aguilar et al., 2010; Heritage et al., 2009; Liu et al., 2007).

A realistic uncertainty propagation is crucial to quantify the precision of a DEM derived from ALS. Additionally, the propagated uncertainty of an airborne lidar-derived DEM is needed for estimating confidence in derived products, e.g., snow volume measured from change detection (Hartzell et al., 2015). The estimation of lidar point uncertainty (i.e., per point error, PPE) has been studied in the literature. However, most previous studies were based on reference points measured by a method other than laser scanning (Hodgson and Bresnahan, 2004), except for a few studies that relied on raw lidar observations (Glennie, 2007; Hartzell et al., 2015). The propagation of uncertainty from the point cloud to a gridded DEM has been studied by a number of published works. However, the majority of these studies accounted for PPE vertical error only (e.g., Aguilar et al., 2010; Kyriakidis and Goodchild, 2006; Shi et al., 2005; Zhu et al., 2005), or both the horizontal and vertical components separately (e.g., Fan et al., 2014). Little work has considered the two components simultaneously (Bui et al., 2022; Skaloud and Schaer, 2012), and in all cases terrain roughness and point density were not considered in the propagation of uncertainty to the final DEM.

The influence of terrain roughness and the density and distribution of data points on the resultant DEM errors have been previously reported, but most of the studies used validation data measured independently by other methods (e.g., Aguilar et al., 2010; Smith et al., 2006; Su and Bork, 2006), except for a few studies which are based on the lidar data itself (Heritage et al., 2009; Milan et al., 2011). In Heritage et al. (2009), various gridded DEMs were generated in the same area by interpolation from terrestrial laser scanning (TLS), EDM theodolite, and aerial lidar

simulated datasets, by which "interpolated" errors were estimated as the difference between each generated DEM and the TLS-based DEM. Averaged "interpolated" error and local terrain roughness, defined by the standard deviation of elevations of all points included, were then calculated on a 0.1-m grid. The "interpolated" errors in this approach included both errors caused by interpolation and measurement error from the TLS and other methods (i.e., EDM theodolite or ALS simulation). In addition, this approach utilized averaged "interpolated" errors rather than their standard deviation, which is more useful in comparison with other studies. The measurement error was also not considered.

To overcome the drawbacks of the method proposed by Heritage et al. (2009), Milan et al. (2011) introduced a method that relies on the relationship between the standard deviation of interpolation errors and local terrain roughness. A linear interpolation was applied to the point cloud dataset by which the "interpolated" error was estimated as the difference between measured and interpolated elevations. At the same time, a 1-m moving window was applied to 0.1-m grids to collect all included points, and local terrain roughness was estimated as the standard deviation of the collected points' elevations. The local terrain roughness at each cloud point was then extracted from these 0.1-m grids. The relationship between the standard deviation of "interpolated" errors and local terrain roughness was established by linear regression for each class of terrain roughness. Finally, at each gridded point, this relationship was applied to estimate its uncertainty. The "interpolated" errors estimated in this approach, and thus their standard deviation, however, includes not only the error caused by interpolation but also the measurement error. This aggregation of measurement and interpolation error does not allow an independent assessment of their individual effects on final DEM accuracy. Additionally, the point density was not considered.

This study proposes a complete approach to estimate laser scanning gridded DEM's uncertainty (i.e., standard deviation), with the objective to derive a reliable uncertainty estimate for gridded DEMs generated by interpolation from ALS-derived point clouds, with no requirement for independent validation measurements. This is a full workflow starting from ALS measurements uncertainties, then considering different error sources caused by interpolation model (TIN in this study) and local influences of terrain roughness and point density. Specifically, this approach is based on: 1) estimated PPE as described by Glennie (2007) and Hartzell et al. (2015), 2) gridded points' interpolated errors

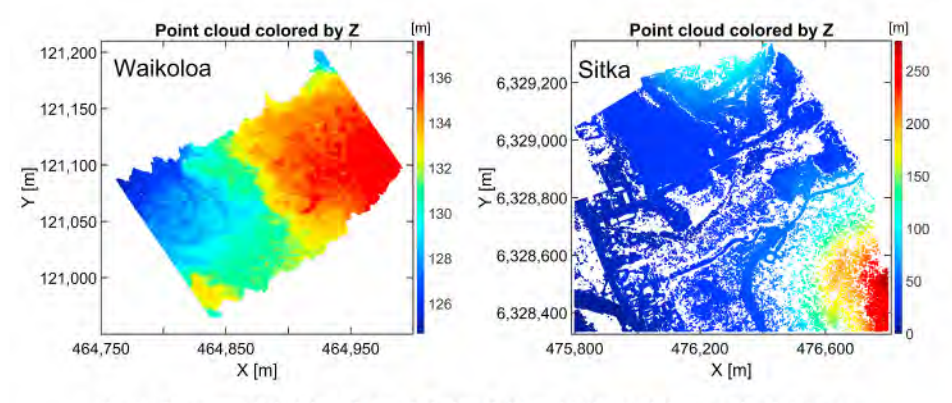


Fig. 2. Topographic heights of the Waikoloa (left) and Sitka (right) point cloud datasets.

propagated from ALS point cloud uncertainty relying on both the horizontal and vertical error components simultaneously developed by Bui et al. (2022), with consideration of both 3) terrain roughness and 4) point density by an improved method based on the initial works in Heritage et al. (2009) and Milan et al. (2011); 1) and 2) have been studied and presented previously while 3) and 4) are presented for the first time; all are incorporated in a unified workflow in this study. TIN interpolation is chosen as the candidate model in this study since it is one of the most widely-used methods, but the proposed approach can be easily modified to work with other interpolation methods (e.g., nearest neighbor, IDW, linear or high-order polynomials).

Unlike Heritage et al. (2009) and Milan et al. (2011) which define local terrain roughness by the standard deviation of elevation for points within a 1-m moving window, in the approach developed here, a local plane is formed by fitting points included in the moving window; local terrain roughness is then estimated as the standard deviation of residuals between points and that plane. This is better because, in TIN interpolation, an interpolation error, and thus its uncertainty, is dependent on how far the interpolated point is away from the plane formed by the three selected points of the TIN triangle, i.e., the distance or height residual between the interpolated point and the terrain surface. Additionally, point density is implicitly dealt with by survey strategy in Heritage et al. (2009); Milan et al. (2011). Here, it is explicitly accounted for by recording the number of points within the moving window. The method developed in this study is tested with ALS datasets, but can also be applied to TLS data as well as 3D data from other methods.

The remainder of the study is organized as follows: the model is introduced in Section 2, the study area and test datasets are given in Section 3. In Section 4, the experimental results are discussed, and Section 5 provides study conclusions.

2. Model development

The quality of a DEM is influenced by various sources, e.g., the accuracy of source data (i.e., lidar measurement errors in this study), errors caused by the interpolation method that is used, and those caused by filtering objects to derive a bare Earth's surface (Fan et al., 2014; Shi et al., 2005; Zhu et al., 2005). In the current study, the vertical uncertainty of a laser scanning-derived gridded DEM is estimated following the steps shown by the workflow in Fig. 1. The uncertainty used throughout this study is the standard deviation (σ) , except for the variance/covariance of cloud points estimated by Step 1.

In Step 1, PPE is estimated for the entire point cloud dataset, based on uncertainties in GNSS-derived position, IMU-based attitude, laser scanner range and angular measurements, boresight angles, and leverarm offsets (Glennie, 2007; Hartzell et al., 2015). Given that for an

ALS based system, ground coordinates (\vec{r}_{σ}^{l}) can be estimated using the laser scanner target coordinate equation (Glennie, 2007), which is given as:

$$\overrightarrow{r}_{G}^{l} = \overrightarrow{r}_{GNSS}^{l} + R_{b}^{l} [R_{s}^{b} \overrightarrow{r}^{s} - \overrightarrow{l}_{b}]$$

$$\tag{1}$$

where, \vec{r}_{GNSS}^l is the GNSS location of the navigation system in the locallevel (l) frame, R_b^l is the inertial navigation system (INS) rotation matrix from body frame (b) to l frame given by the rotation angles ω , φ , κ , R_s^b is the rotation of the scanner (s) frame to the INS b frame (also referred to as the boresight matrix, given by angles $d\omega$, $d\varphi$, $d\kappa$), \vec{r}^s are the coordinates of the ground point in the laser scanner coordinate frame and \vec{l}_b is the offset from the navigation system origin to the scanner origin (lever-arm).

All parameters on the right hand side of Equation (1) are observed, and therefore contain errors. We can examine the effects of these errors by truncating a Taylor Series expansion of Equation (1) after the first term:

$$\begin{bmatrix} \delta X \\ \delta Y \\ \delta Z \\ \delta Z \end{bmatrix}_{G}^{l} = \begin{bmatrix} \delta X \\ \delta Y \\ \delta Z \\ \delta Z \end{bmatrix}_{GANS}^{l} + A \begin{bmatrix} \delta \omega \\ \delta \varphi \\ \delta \kappa \end{bmatrix} + B \begin{bmatrix} \delta d\omega \\ \delta d\varphi \\ \delta d\kappa \end{bmatrix} + C \begin{bmatrix} \delta x_{s} \\ \delta y_{s} \\ \delta z_{s} \end{bmatrix}^{s} + D \begin{bmatrix} \delta l_{x} \\ \delta l_{y} \\ \delta l_{y} \\ \delta l_{z} \end{bmatrix}$$
(2)

where the matrices **A**, **B**, **C** and **D** are the Jacobians of the transformation and contain partial derivatives of the ground coordinates with respect to the unknown coordinates as:

$$A = \left[\frac{\delta \overrightarrow{r}_{G}^{l}}{\delta \omega} \frac{\delta \overrightarrow{r}_{G}^{l}}{\delta \varphi} \frac{\delta \overrightarrow{r}_{G}^{l}}{\delta \kappa} \right], B = \left[\frac{\delta \overrightarrow{r}_{G}^{l}}{\delta d \omega} \frac{\delta \overrightarrow{r}_{G}^{l}}{\delta d \varphi} \frac{\delta \overrightarrow{r}_{G}^{l}}{\delta d \kappa} \right], C$$

$$= \left[\frac{\delta \overrightarrow{r}_{G}^{l}}{\delta x_{x}} \frac{\delta \overrightarrow{r}_{G}^{l}}{\delta y_{x}} \frac{\delta \overrightarrow{r}_{G}^{l}}{\delta z_{x}} \right], D = \left[\frac{\delta \overrightarrow{r}_{G}^{l}}{\delta l_{x}} \frac{\delta \overrightarrow{r}_{G}^{l}}{\delta l_{y}} \frac{\delta \overrightarrow{r}_{G}^{l}}{\delta l_{z}} \right]$$
(3)

Using Equation (2), we can input estimated errors for the GNSS/INS navigation system, laser scanner assembly and platform calibration and estimate uncertainty in the resultant laser scanning ground point coordinates. For additional details the reader is referred to Glennie (2007) or Schaer et al. (2007).

The propagated uncertainty for the gridded DEM due to interpolation is then estimated from the point cloud uncertainty in Step 2. Here, the general law of propagation of variances (GLOPOV) is adopted with both horizontal and vertical components of point cloud uncertainty considered simultaneously, together with their correlation. The propagated uncertainty σ_{prop_p} of a gridded point P with coordinates x_p , y_p , z_p can be estimated as (Bui et al., 2022):

$$\sigma_{prop_p}^2 = \left[\frac{\partial z_p}{\partial x_1} \frac{\partial z_p}{\partial y_1} \frac{\partial z_p}{\partial z_1} \cdots \frac{\partial z_p}{\partial z_3}\right] \times \begin{bmatrix} \sigma_{x_1}^2 & \sigma_{x_1y_1} & \sigma_{x_1z_1} & \cdots & \sigma_{x_1z_3} \\ \sigma_{y_1x_1} & \sigma_{y_1}^2 & \sigma_{y_1z_1} & \cdots & \sigma_{y_1z_3} \\ \sigma_{z_1x_1} & \sigma_{z_1y_1} & \sigma_{z_1}^2 & \cdots & \sigma_{z_1z_3} \\ \vdots & \vdots & \vdots & \ddots & \vdots \\ \sigma_{z_3x_1} & \sigma_{z_3y_1} & \sigma_{z_3z_1} & \cdots & \sigma_{z_3}^2 \end{bmatrix} \times \begin{bmatrix} \frac{\partial z_p}{\partial x_1} \\ \frac{\partial z_p}{\partial y_1} \\ \frac{\partial z_p}{\partial z_1} \\ \vdots \\ \frac{\partial z_p}{\partial z_3} \end{bmatrix}$$

$$(4)$$

where $\frac{\partial z_p}{\partial x_i}$, $\frac{\partial z_p}{\partial y_i}$, and $\frac{\partial z_p}{\partial z_i}$ (i=1,2,3) are the partial derivatives of z_p w.r.t the coordinates of the corresponding triangle's vertices, $\sigma_{x_i}^2$, $\sigma_{y_i}^2$, and $\sigma_{z_i}^2$ are the variances of the uncertainty in the coordinates of the triangle's vertices, $\sigma_{x_iy_i}$, $\sigma_{x_iz_i}$, $\sigma_{y_iz_i}$ (i=1,2,3), and $\sigma_{x_ix_j}$, $\sigma_{x_iy_j}$, $\sigma_{x_iz_j}$, $\sigma_{y_iy_j}$, $\sigma_{y_iz_i}$, $\sigma_{z_iz_j}$, σ

because interpolation error is dependent on how far away the interpolated point is from the plane formed by the three points of the TIN triangle. Therefore, in the case of a steep surface, a high σ_z will exist but a smaller interpolated error may be computed if the interpolated point is close to the TIN triangle; giving a smaller σ_Δ .

The entire point cloud dataset is split into interpolated and remaining datasets; we generated 1-m regular grids, then an interpolated dataset is formed by selecting only cloud points closest to the 1-m grid intersections. For each interpolated point in the interpolated dataset, a moving window is then centered at the point, and the σ_z of all points from the remaining dataset located within the moving window is calculated. For the planar estimate of terrain roughness, a least squares planar fit of the remaining points within the moving window is formed, the residuals of the points (z_r) with respect to the best-fit plane are estimated, by which the standard deviation of the residuals (σ_{z_r}) is computed. Simultaneously, point density (ρ) is also estimated by dividing the number of remaining cloud points within the moving widow by the area of the window, and used to compute terrain roughness/point density (σ_z/ρ) and σ_{z_r}/ρ). TIN interpolation is then used to

$$\frac{\partial z_p}{\partial x_1} = \frac{1}{F^2} \{ (y_3 - y_2) x_p A + (y_3 - y_2) y_p B + (y_3 - y_2) E + [(z_2 - z_3) y_p + (y_2 z_3 - y_3 z_2)] F \}
\frac{\partial z_p}{\partial x_2} = \frac{1}{F^2} \{ (y_1 - y_3) x_p A + (y_1 - y_3) y_p B + (y_1 - y_3) E + [(z_3 - z_1) y_p + (y_3 z_1 - y_1 z_3)] F \}
\frac{\partial z_p}{\partial x_3} = \frac{1}{F^2} \{ (y_2 - y_1) x_p A + (y_2 - y_1) y_p B + (y_2 - y_1) E + [(z_1 - z_2) y_p + (y_1 z_2 - y_2 z_1)] F \}
\frac{\partial z_p}{\partial y_1} = \frac{1}{F^2} \{ (x_2 - x_3) x_p A + (x_2 - x_3) y_p B + (x_2 - x_3) E + [(z_3 - z_2) x_p + (x_3 z_2 - x_2 z_3)] F \}
\frac{\partial z_p}{\partial y_2} = \frac{1}{F^2} \{ (x_3 - x_1) x_p A + (x_3 - x_1) y_p B + (x_3 - x_1) E + [(z_1 - z_3) x_p + (x_1 z_3 - x_3 z_1)] F \}$$

$$\frac{\partial z_p}{\partial y_3} = \frac{1}{F^2} \{ (x_1 - x_2) x_p A + (x_1 - x_2) y_p B + (x_1 - x_2) E + [(z_2 - z_1) x_p + (x_2 z_1 - x_1 z_2)] F \}$$

$$\frac{\partial z_p}{\partial z_1} = \frac{1}{F} [(y_2 - y_3) x_p + (x_3 - x_2) y_p + (x_2 y_3 - x_3 y_2)]$$

$$= \frac{1}{F} [(y_3 - y_1) x_p + (x_1 - x_3) y_p + (x_3 y_1 - x_1 y_3)]$$

$$= \frac{1}{F} [(y_1 - y_2) x_p + (x_2 - x_1) y_p + (x_1 y_2 - x_2 y_1)]$$

where A, B, C, and E are the coefficients for TIN interpolation, which are:

$$A = y_1 z_3 - y_1 z_2 + y_2 z_1 - y_2 z_3 + y_3 z_2 - y_3 z_1$$

$$B = x_1 z_2 - x_1 z_3 + x_2 z_3 - x_2 z_1 + x_3 z_1 - x_3 z_2$$

$$E = x_1 y_2 z_3 - x_1 y_3 z_2 + x_2 y_3 z_1 - x_2 y_1 z_3 + x_3 y_1 z_2 - x_3 y_2 z_1$$

$$F = x_1 y_2 - x_1 y_3 + x_2 y_3 - x_2 y_1 + x_3 y_1 - x_3 y_2$$
(6)

In Step 3, the relationship between point cloud uncertainty, terrain roughness, and point density is established. Terrain roughness is expected to affect interpolation errors, and thus uncertainty, in such a way that higher terrain roughness will result in higher interpolation uncertainties (Heritage et al., 2009; Milan et al., 2011; Wheaton et al., 2010). Conversely, higher point density is expected to result in lower interpolated uncertainties (Liu et al., 2007). Here, two estimates of terrain roughness are computed and compared. The first is based on the approach presented in Heritage et al. (2009) and Milan et al. (2011), which is defined by local surface variability represented by the standard deviation of point heights (σ_z) located within a moving window. The second is defined by the standard deviation of point residual deviations with respect to a least squares planar fit of points within a moving window ($\sigma_{\rm gr}$). This second measure of terrain roughness is proposed

compute the heights of points in the interpolated dataset from the remaining dataset and "interpolation" errors (Δ_z) are computed as the difference between the interpolated and measured heights. The relationship between the standard deviation of interpolation error (σ_Δ) and terrain roughness/point density is established; σ_z/ρ and σ_{z_r}/ρ are binned into regular groups. In each group, all interpolation points with σ_z/ρ and σ_{z_r}/ρ lying within a pre-determined range are gathered. Then, σ_Δ and the mean σ_z/ρ and σ_{z_r}/ρ are computed for each bin. Results for these calculations are provided in Sections 4.1–4.2.

The uncertainty propagation with TIN interpolation in Step 2 is based on the assumption that the surface represented by the three points used to form a TIN triangle is a plane. However, in practice, this may not be the case, and deviation from planar is dependent on both terrain roughness and sample point density. Therefore, the relationship between point cloud uncertainty and both terrain roughness and point density derived from Step 3 is used in Step 4 to scale the GLOPOV propagated uncertainty estimated in Step 2. In this way, the final uncertainty of the gridded DEM is calculated. A linear relationship between terrain roughness/point density and the standard deviation of interpolated errors found in Step 3 is anticipated as:

Table 1 Statistics of point cloud uncertainty (unit: m^2).

Variance/Covariance	$\sigma_{x,ppg}^2$	$\sigma_{xy,ppE}$	$\sigma_{xx,ppE}$	$\sigma_{y,PPE}^2$	$\sigma_{yz,PPE}$	$\sigma_{z,ppg}^2$
Waikoloa					-	
Minimum	0.003	-0.004	-0.003	0.003	-0.004	0.010
Maximum	0.009	0.001	0.002	0.012	0.003	0.013
Mean	0.003	0	0	0.003	0	0.010
Sitka						
Minimum	0.006	-0.005	-0.003	0.005	-0.003	0.010
Maximum	0.016	0	0.003	0.015	0.003	0.013
Mean	0.010	-0.001	0	0.010	0	0.011

$$\sigma_{\Delta} = b + n \frac{\sigma_{z_r}}{\rho} \tag{7}$$

where b is the y-intercept and n is the slope. Actually, b is close, but not exactly the standard deviation of interpolated errors at zero terrain roughness/point density σ_{Δ}^{o} . Therefore, we modify the relationship shown in Equation (7) by replacing b by σ_{Δ}^{o} so that we have:

$$\frac{\sigma_{\Delta}}{\sigma_{\Delta}^{q}} = 1 + m \frac{\sigma_{z_{r}}}{\rho}$$
(8)

where $m=\frac{n}{\sigma_{\Lambda}^{2}}$ is the slope/y-intercept fraction. The relationship shown in Equation (8) is of a modified linear format developed in such a way to guarantee that, if the fraction $\frac{\sigma_{N}}{\rho}$ equals zero (i.e., no terrain roughness) then the estimation of σ_{Δ} is exactly the zero-roughness uncertainty σ_{Δ}^{0} .

Equation (B) is applied to σ_{Δ} and the mean $\frac{\sigma_{s_r}}{\rho}$ found in Step 3 to estimate m, which can be applied to scale the gridded propagated uncertainty estimated in Step 2. To this end, the fraction $\frac{\sigma_{s_r}}{\rho}$ at each gridded point is needed. A 1-m moving window is applied to compute terrain roughness (σ_{z_r}) and point density (ρ) using all cloud points within the window. The fraction $\frac{\sigma_{s_r}}{\rho}$ is then calculated and the scale factors can be

estimated for all gridded points as:

$$scale = 1 + m \frac{\sigma_{z_t}}{a}$$
(9)

The final gridded DEM uncertainty is then calculated as:

$$\sigma_{DEM} = \sigma_{prop} \times scale \tag{10}$$

where σ_{prop} is the propagated uncertainty of the gridded DEM found in Step 2 (Equation (4)).

3. Study areas and test datasets

Two lidar datasets at Waikoloa, Hawaii and Sitka, Alaska are used in this study to test the full workflow proposed in Fig. 1. The former is an airborne lidar dataset collected by an uncrewed aerial vehicle near Waikoloa, Hawaii, U.S in September 2019 over volcanic lava fields. The measurements were made with a Riegl VUX-1UAV laser scanner mounted on a Riegl RiCopter operating at approximately 50 m above ground level. The horizontal datum is NAD83(PA11) Hawaii State Plane Coordinate System Zone 1; the elevations are ellipsoidal. The geographic location and distribution of the dataset is shown in Fig. 2 (left). A total of 399,179 points are included in the dataset covering an area of \sim 35, 000 m², with topographic heights of the points ranging between \sim 125 m and \sim 138 m, with a mean value of \sim 132 m. The terrain consists of complex pahoehoe lava flow formations with scattered low vegetation.

The propagated uncertainty (i.e., per point error; PPE) of the point cloud dataset was estimated using the approach described in Glennie (2007) and Hartzell et al. (2015) (Step 1 in Fig. 1). This is calculated from known lidar error sources, including uncertainties from GNSS-based position, IMU-derived attitude, laser scanner's range and angular measurements, boresight angles, and lever-arm offsets. A summary of point cloud uncertainty statistics is shown in Table 1 (maximum, minimum, and mean values); these include the uncertainty

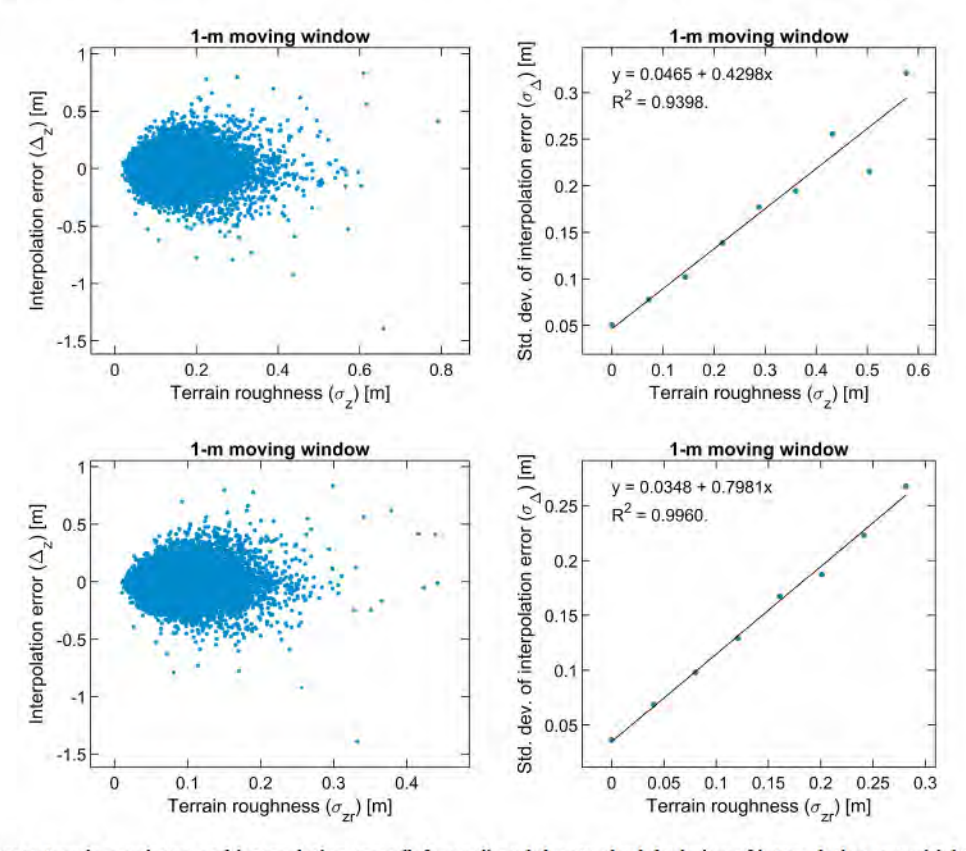


Fig. 3. Relationship between terrain roughness and interpolation error (left panel) and the standard deviation of interpolation error (right panel) for the Waikoloa dataset. Terrain roughness is defined as the standard deviation of height (top panel) and standard deviation of planar residuals (bottom panel).

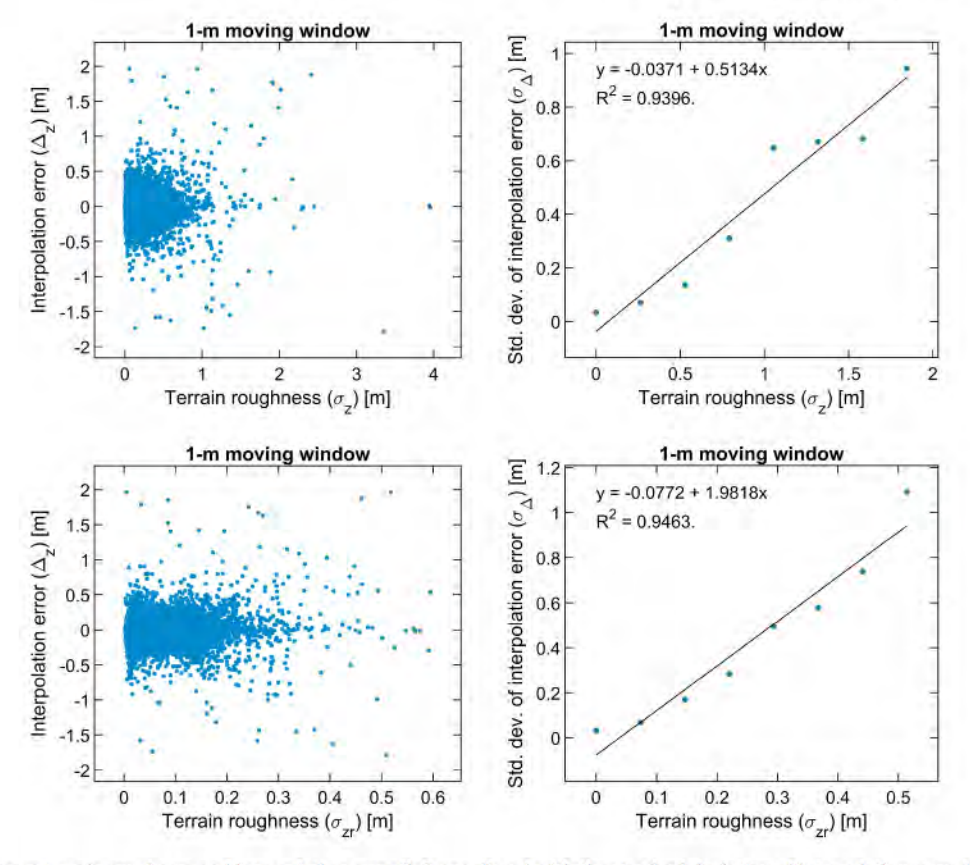


Fig. 4. Relationship between terrain roughness and interpolation error (left panel) and with the standard deviation of interpolation error (right panel) for the Sitka dataset. Terrain roughness is defined as the standard deviation of height (top panel) and standard deviation of planar residual (bottom panel).

in both horizontal and vertical components and their correlation at each cloud point. We note that the uncertainty correlation in the X, Y, Z coordinate components is computed for each point, but the correlation between points is not available.

The second dataset is a helicopter-based lidar collection over a high-relief terrain area near Sitka, Alaska in May 2016. The measurements were made by a system combining a Riegl VQ-480i laser scanner with a iXBlue ATLANS-C inertial measurement unit, mounted on a Robinson R44 Raven II helicopter flying at roughly 500 m above ground level. The reference coordinate system is NAD83(2011) epoch 2010.00; the elevations are ellipsoidal heights with respect to WGS84 (World Geodetic System 1984) (DMA, 1987, 1991). The geographic location and distribution of the dataset is shown in Fig. 2 (right). A total of 2,580,894 points are included in the dataset covering an area of 1 km², with

topographical heights of the points ranging between ~ 0 m and ~ 278 m with a mean value of ~ 38 m. A summary of point cloud uncertainty statistics is shown in Table 1 (maximum, minimum, and mean values); these include the uncertainty in the horizontal and vertical components and their correlation at each cloud point. Like the Waikoloa dataset, the uncertainty correlation in the X, Y, Z coordinate components is computed for each point, but the correlation between points is not available.

4. Results and discussion

4.1. Influence of terrain roughness on TIN interpolated errors

The influence of terrain roughness on TIN interpolation is assessed in

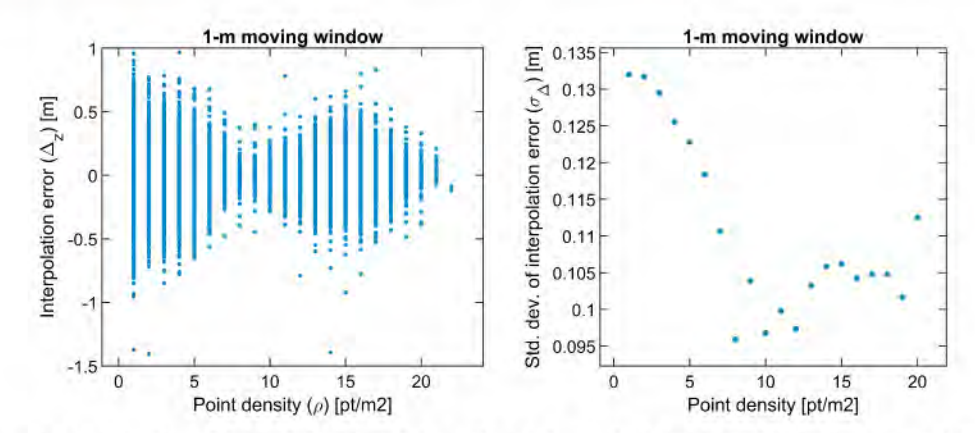


Fig. 5. Relationship between point density and interpolation error (left panel) and the standard deviation of interpolation error (right panel) for the Waikoloa dataset.

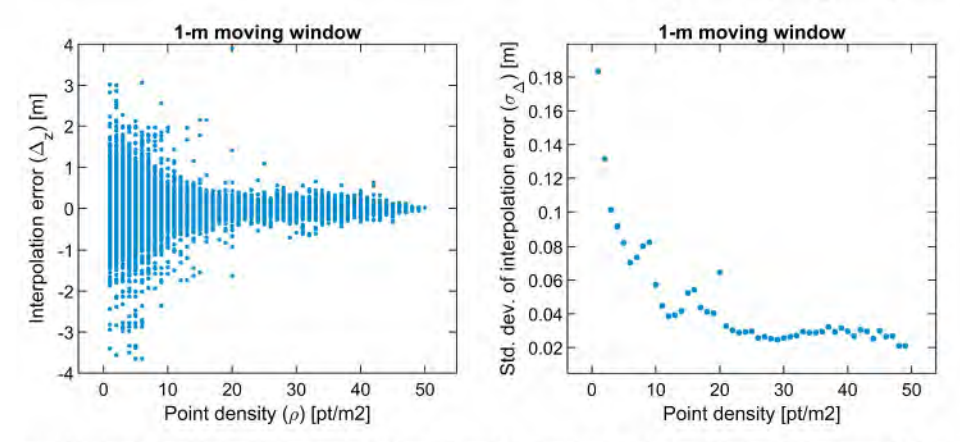


Fig. 6. Relationship between point density and interpolation error (left panel) and the standard deviation of interpolation error (right panel) for the Sitka dataset.

this section with a moving window of different sizes from 1 m to 10 m to determine the best window size. Interpolation error versus terrain roughness with a 1-m moving window is shown in Fig. 3 (top-left) and the relationship between binned σ_{Δ} and σ_{z} is shown in Fig. 3 (top-right). Regression is then applied to evaluate the linear relationship between σ_{Δ} and σ_{z} , with a coefficient of determination (R^{2}) of 0.9398. A good correlation between σ_{Δ} and σ_{z} is displayed in Fig. 3 (top-right). However, more precisely, interpolation error is dependent on how far away the interpolated point is from the plane formed by the three points of the TIN triangle. Therefore, in the case of a steep surface, a high σ_{z} will exist but a smaller Δ_{z} may be computed if the interpolated point is close to the TIN triangle; giving a smaller σ_{Δ} . In this case, $\sigma_{z_{r}}$ is expected to be a better representation of terrain roughness.

The relationship between Δ_z and σ_{z_r} is shown in Fig. 3 (bottom-left) for the same dataset, and unsurprisingly the range of σ_{z_r} is smaller than that of σ_z (cf. top-left panel of Fig. 3). Fig. 3 (bottom-right) shows the relationship between binned σ_Δ and σ_{z_r} . Linear regression is applied to the relationship between σ_Δ and σ_{z_r} with a higher coefficient of determination (0.9960). With the consideration of the combined influence of terrain roughness and point density, a comparison of the influence of terrain roughness with different moving windows is not shown here. Rather, a detailed comparison will be provided in Section 4.3.

The same approach was tested with the Sitka dataset. The results derived from moving windows with sizes from 1 m to 10 m are analyzed. The comparison between interpolation error and terrain roughness defined by σ_z and σ_z , for the 1-m moving window are shown in Fig. 4 (left), from which the relationship between the standard deviation of interpolation error (σ_Δ) with σ_z and σ_{z_r} is established (Fig. 4, right). Regression is then applied to evaluate how σ_Δ is linearly associated with both σ_z and σ_{z_r} . Like the Waikoloa data, coefficients of determination (R^2) are higher for σ_{z_r} (0.9463) than σ_z (0.9396), while the range of terrain roughness is larger in the σ_z case (up to 4 m) than the σ_z , case

(around 0.6 m). While the fits in Figs. 3 and 4 show high coefficients of determination, the slopes and intercepts for the lines are not the same for each dataset. The differences are primarily due to the different point densities of the datasets, which will be addressed in Section 4.3.

4.2. Influence of point density on TIN interpolated errors

In this section, the influence of point density on TIN interpolation errors is investigated. The relationship between interpolation error and point density (ρ) is examined by using a moving window of different sizes from 1 m to 10 m. Changes in point density are examined by reselecting the remaining points closest to varying grids of 0.5 × 0.5, 0.75 × 0.75, and 1.0 × 1.0 m, together with the original remaining point cloud dataset. For each case, the interpolated heights are calculated from the re-selected dataset to calculate interpolation errors, and point densities are then re-estimated. The relationship between Δ_z and ρ is shown in Fig. 5 (left) for the Waikoloa dataset. The point density is then binned into 1-pt/m² steps and σ_Δ is computed for each bin. The relationship between ρ and σ_Δ for the 1-m window case is shown in Fig. 5 (right).

Generally, higher point density corresponds to lower interpolation uncertainties as shown in Fig. 5. The relationship holds for a point density range between 1 and 8 points/m² (see Fig. 5, right). Beyond this range, the uncertainty slightly increases with an increase in point density; this is likely caused by a number of reasons. The first is the varying effects of horizontal uncertainty. In the case of a high point density (i.e., more than 8 points/m² in this experiment), the surface represented by the TIN triangles can be much steeper than in the case of lower point density (i.e., fewer than 8 points/m²). Therefore, the influence of point cloud horizontal uncertainties is more significant. We note here that the uncertainty of a point interpolated from a point cloud using a TIN is dependent on the uncertainty of the point cloud, the location of the

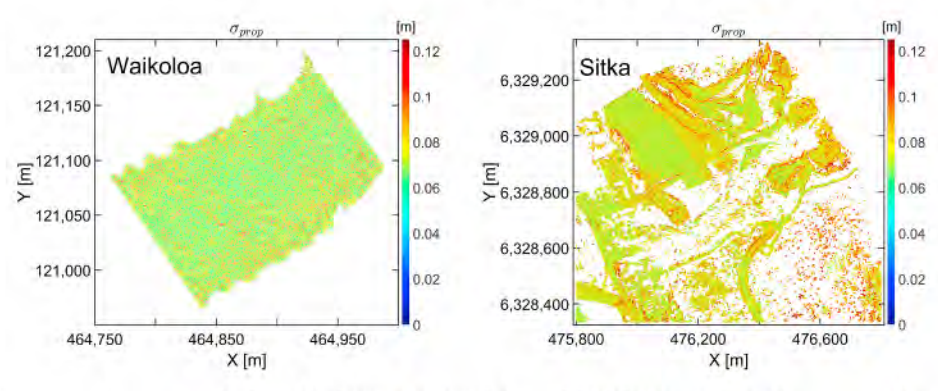


Fig. 7. GLOPOV propagated uncertainty for the gridded DEM: (left) Waikoloa and (right) Sitka. Gaps in Sitka are caused by dense vegetation.

Table 2 Statistics of GLOPOV propagated uncertainty (σ_{prop}) for the gridded DEM (units: m).

Dataset	Minimum	Maximum	Mean	
Waikoloa	0.059	0.122	0.072	
Sitka	0.059	0.301	0.079	

interpolated point within the selected triangle, and the slope of the triangle (Bui et al., 2022). Both the horizontal and vertical uncertainties are almost identical between cloud points (see Table 1), so the first influence is almost equivalent regardless of which points are selected to form the TIN triangle. The second influence alters the magnitude of uncertainty at the interpolated point, which is bounded between 1/3 and 1 of the vertical uncertainty (Bui et al., 2022). The influence of point cloud horizontal uncertainty is very high for high-slope surfaces, and thus can be dominant for high point density. Additionally, terrain roughness may also influence the results shown in Fig. 5.

The same approach was applied to the Sitka dataset. The relationship between ρ and Δ_z for a 1-m moving window is shown in Fig. 6 (left) and between ρ and σ_Δ is shown in Fig. 6 (right). A similar result to the Waikoloa data is presented; higher point density corresponds to lower uncertainties. In particular, σ_Δ reduces quickly with the increase of ρ from 1 point/m² (\sim 0.183 m) to 20 point/m² (\sim 0.064 m). Again, a comparison of the influence of point density with different moving windows is not shown here. Instead, a detailed comparison of the combined influence of terrain roughness and point density (σ_{z_r}/ρ) will be given in Section 4.3 for varied window sizes.

4.3. Uncertainty of a gridded DEM considering both terrain roughness and point density

The workflow presented in Fig. 1 is employed to derive the uncertainty of gridded DEMs. Point cloud uncertainties were estimated in Step 1 as shown in Section 3 (Table 1). In Step 2, gridded point propagated uncertainty (σ_{prop}) at 1-m spacing was estimated from point uncertainty and their correlation from Step 1 by Equation (4) (see Table 1). Fig. 7 shows this propagated uncertainty for both datasets with their statistics (maximum, minimum, and mean values) given in Table 2. Although point cloud uncertainty is approximately identical between points (see Table 1), the propagated uncertainty at the gridded points varies with a mean value of 0.072 m (Waikoloa) and 0.079 m (Sitka) and a maximum value of 0.122 m (Waikoloa) and 0.301 m (Sitka). This wide range in the resultant propagated uncertainty is attributed to the varying influence of point cloud horizontal uncertainty on gridded point propagated uncertainty, which varies according to the magnitude of the slope of the TIN triangle (Fan et al., 2014; Hodgson and Bresnahan, 2004) (Further details on this can be found from Bui et al. (2022)).

The individual influences of σ_{z_r} and ρ on point cloud uncertainty have been evaluated in Sections 4.1–4.2. In this section, their combined influence is investigated and applied to the propagated gridded DEM uncertainty. The same methods and datasets in Sections 4.1–4.2 are used here. The fraction $\frac{\sigma_{z_r}}{\rho}$ is computed for all points in the interpolated dataset, and a plot showing its relationship with TIN interpolation error corresponding to the 1-m moving window is shown in Fig. 8 (left). The results are then binned into regular groups of $\frac{\sigma_{z_r}}{\rho}$. In each bin, a standard deviation of interpolation error and the mean terrain roughness/point density are computed with the results shown in Fig. 8 (right). A linear-fit is then applied to estimate the slope with estimated coefficients of determination of 0.9822 (Waikoloa) and 0.9596 (Sitka).

The y-intercepts of the linear-fit regressions shown in Fig. 8 (right)

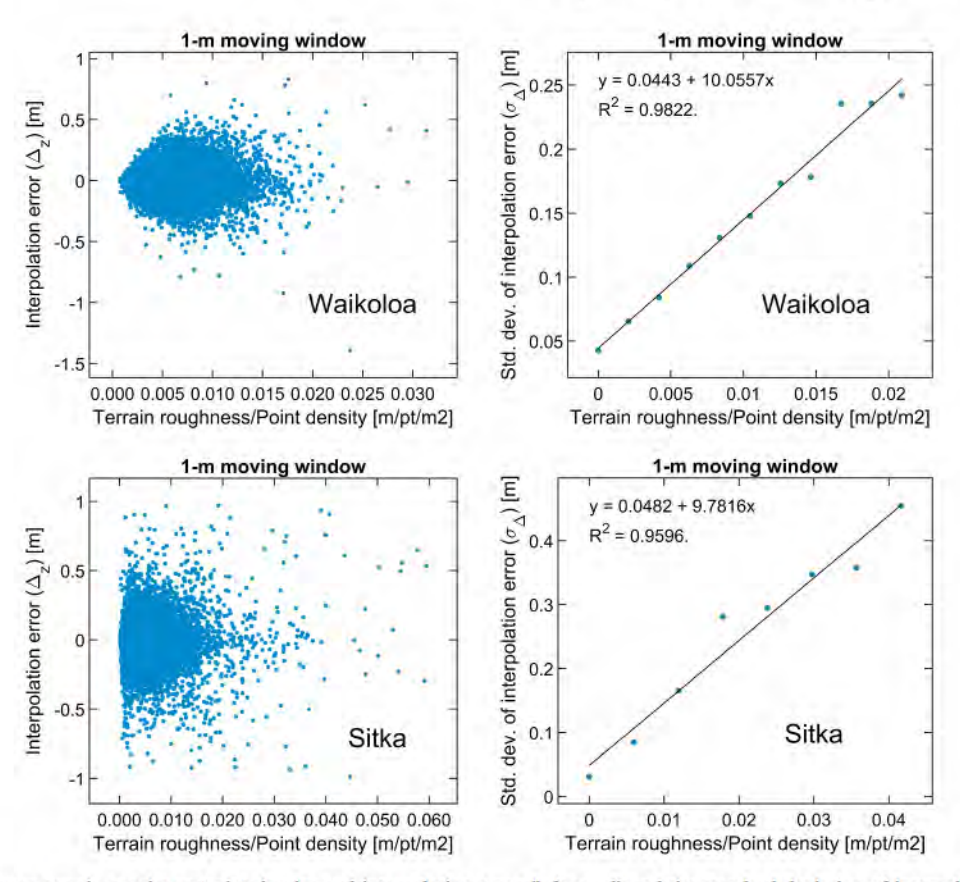


Fig. 8. Relationship between terrain roughness/point density and interpolation error (left panel) and the standard deviation of interpolation error estimated for points binned by terrain roughness/point density (right panel): (top panel) Waikoloa and (bottom panel) Sitka.

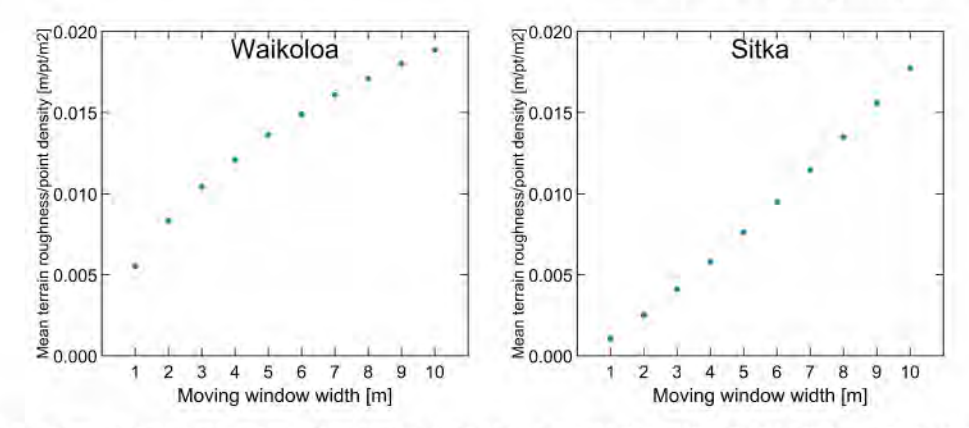


Fig. 9. Change in the mean terrain roughness/point density with moving window size: (left) Waikoloa and (right) Sitka.

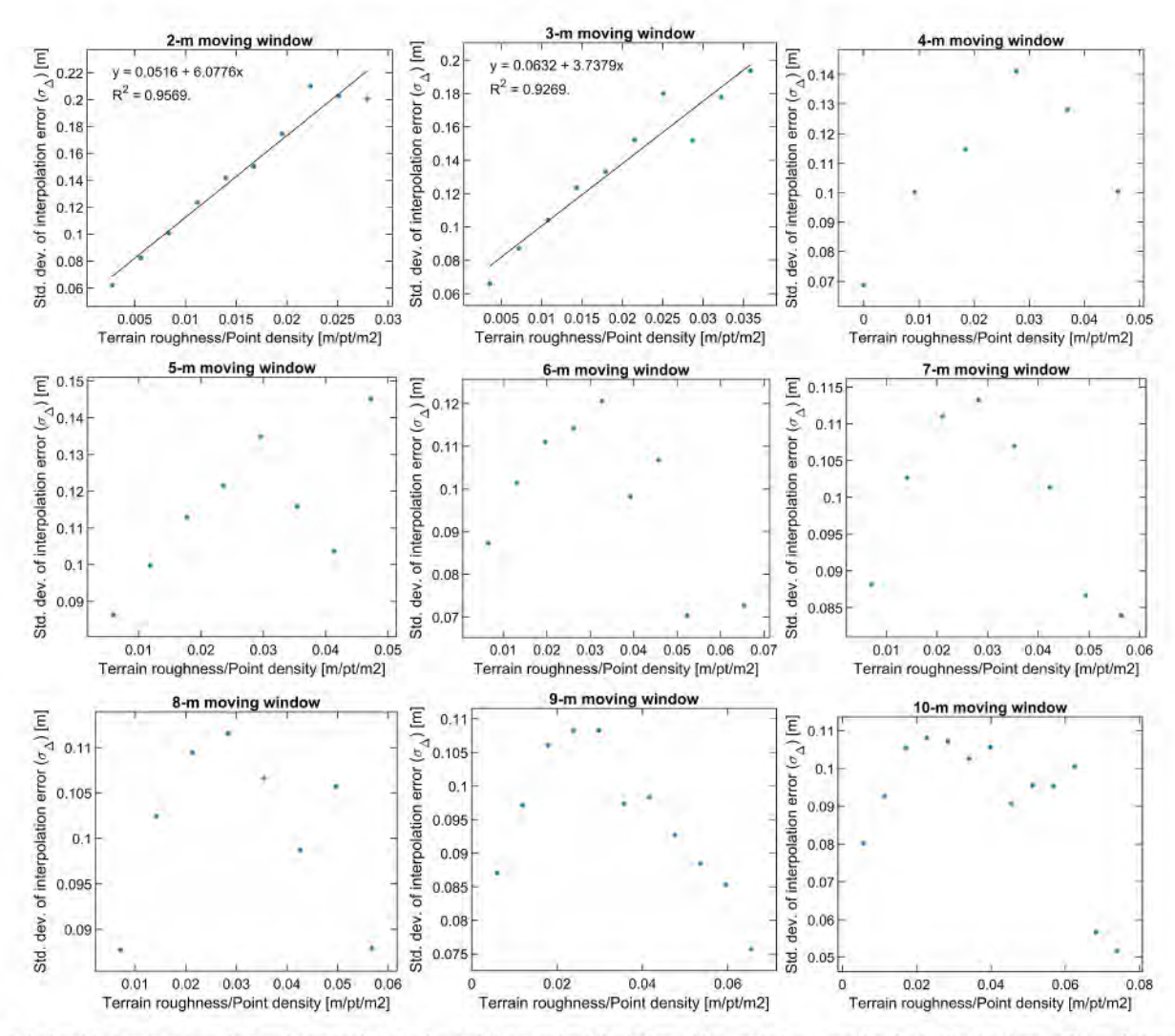


Fig. 10. Relationship between terrain roughness/point density and the standard deviation of interpolation error for the Waikoloa dataset for varied moving window sizes

reflect the uncertainty with zero terrain roughness, and the slopes reflect the added uncertainty caused by nonzero terrain roughness/point density. Ideally, the slope of the line should be dataset independent. As shown in previous studies (Bui et al., 2022; Fan et al., 2014; Hu et al., 2009), with a horizontal TIN face and without considering terrain roughness/point density, the propagated error variance of interpolated points is expected to be bounded within one-third and one PPE error

variance ($\sigma_{z,PPE}^2$ in Table 1), depending on the location of the interpolated point with respect to the TIN vertices. As a result, the corresponding expected range of the standard deviation of interpolation errors is between 0.058 m and 0.100 m. The zero terrain roughness/point density uncertainty estimates shown in Fig. 8 (right) are 0.044 m with the Waikoloa dataset and 0.048 m with the Sitka dataset, which appear to be underestimated compared to the expected range.

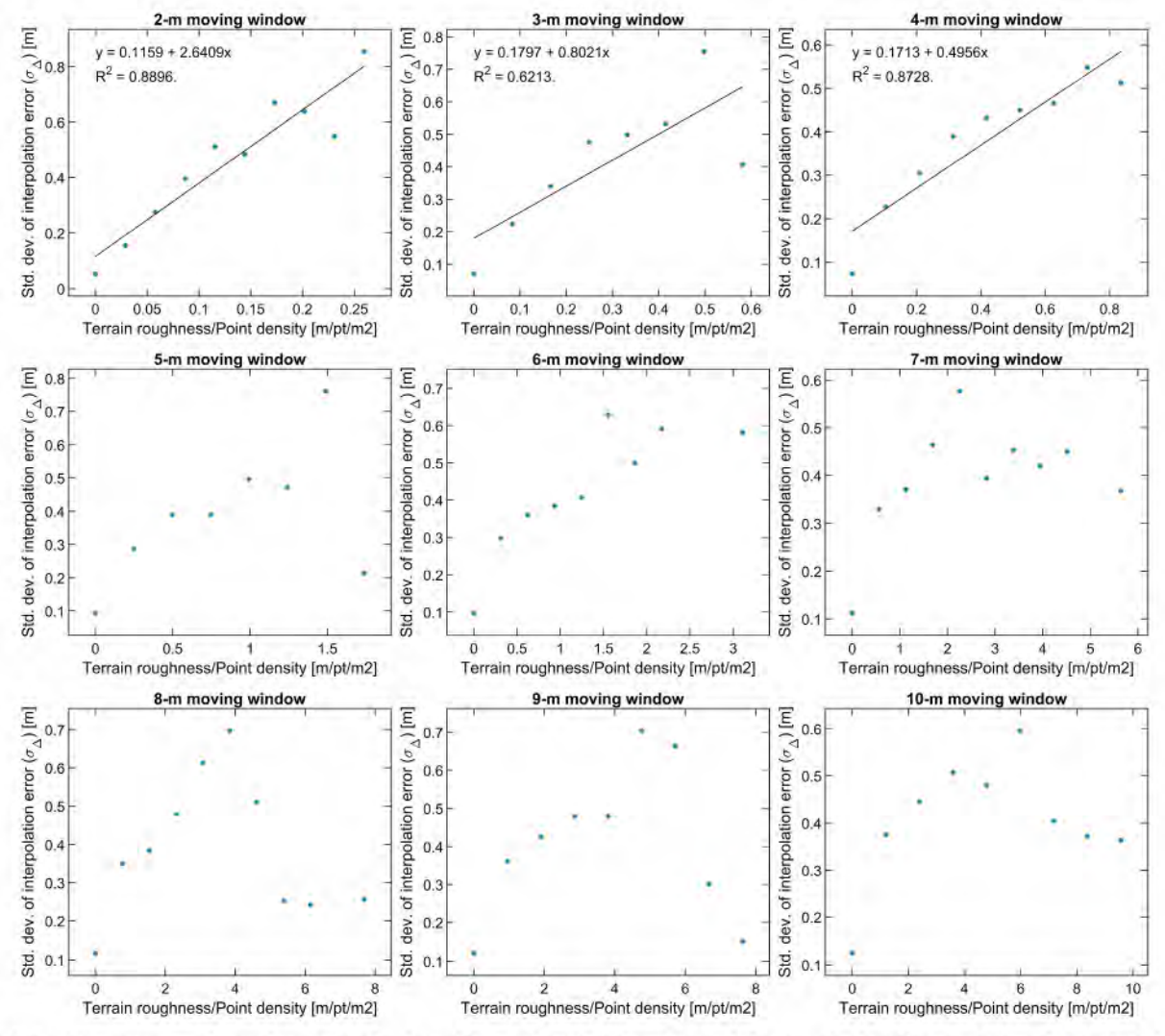


Fig. 11. Relationship between terrain roughness/point density and the standard deviation of interpolation error for the Sitka dataset for varied moving window sizes.

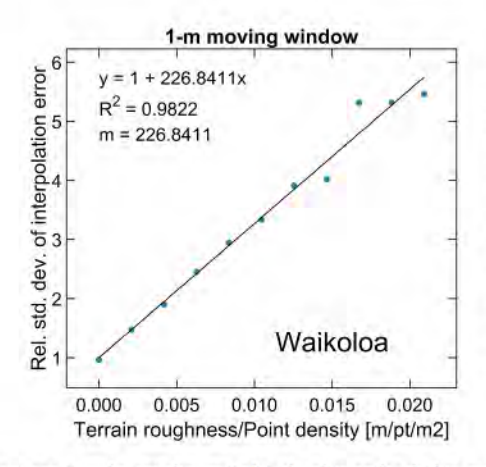
This is due to the fact that, by definition, the uncertainty is the standard deviation of the interpolation errors—the differences between the interpolated heights and the true or the most probable values (Ghilani and Wolf, 2010), which was used in PPE uncertainty estimation using expected uncertainties of lidar measurements (Table 1). However, the true or the most probable heights are not available with the cloud points, and the "interpolation" errors were computed as the differences between interpolated and measured heights (Fig. 8). We note that these estimated nonzero terrain roughness/point density uncertainties are not directly applied in the proposed workflow. Instead, the relationship between nonzero and zero terrain roughness/point density uncertainties shown in Equation (8) is applied, which is assumed to be consistent between the two approaches.

In this study, terrain roughness and point density are defined as the standard deviation of residual height and the number of points located within a moving window. Here, we examine these same quantities with moving windows of different sizes from 1 m to 10 m. The results indicate that, in general, a larger moving window leads to a higher estimate of terrain roughness. In contrast, because of the spatially-regular sampling by airborne lidar, only small changes in the point density are observed for varied window sizes. As a result, the fraction terrain roughness/point density increases with an increase in window size. Fig. 9 shows the mean terrain roughness/point density computed for varied moving window sizes. The results show an increase in the mean terrain roughness/point density from 0.006 m³/pt (Waikoloa) and 0.001 m³/pt (Sitka) for a 1-m

moving window to 0.019 $\rm m^3/pt$ (Waikoloa) and 0.018 $\rm m^3/pt$ (Sitka) for a 10-m moving window.

Fig. 10 shows the relationship between terrain roughness/point density and the standard deviation of interpolation error for moving window sizes from 2 m to 10 m, for the Waikoloa dataset. In comparison with Fig. 8 (top-right) that shows a linear relationship with a high correlation coefficient, Fig. 10 does not show as good a linear correlation, particularly for windows larger than 3 m. This is likely due to a decorrelation between terrain roughness estimated using large windows and TIN interpolation error; a larger window results in higher terrain roughness/point density (see Fig. 9), but no change in interpolation error. For TIN interpolation, the height of a point is interpolated from a triangle generated using three surrounding points, and the 'interpolation error' is the vertical distance between the actual point measured on the surface and that projected from the point to the plane formed by the TIN triangle. Therefore, the uncertainty of a point is dependent on the 'local' roughness, i.e., the roughness defined by near points rather than far ones. With the current dataset, a 1-m moving window appears most appropriate and is thus chosen for further examination.

Fig. 11 shows the relationship between terrain roughness/point density and the standard deviation of interpolation error with different moving window sizes for the Sitka dataset. By comparing Fig. 8 (bottom-right) and Fig. 11, it can be seen that the 1-m moving window has the highest R^2 (0.9596). Therefore, a 1-m moving window was selected for further analysis. A clear nonlinear trend can be found in moving



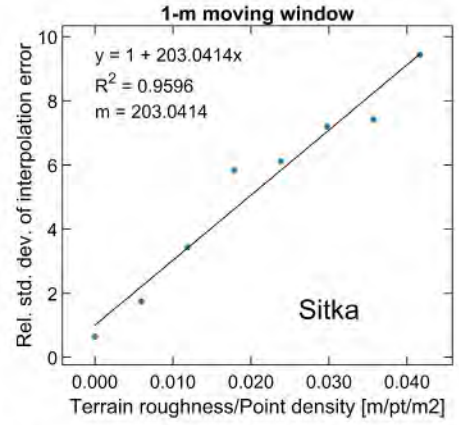


Fig. 12. Relationship between terrain roughness/point density and relative standard deviation of interpolation error estimated for points binned by terrain roughness/point density (left) Waikoloa and (right) Sitka.

Table 3 Statistics of scale, propagated and final uncertainty.

Statistics	Waikoloa			Sitka		
	scale	σ _{prop} [m]	σ _{DEM} [m]	scale	<u>σ_{prop}</u> [m]	σ _{DEM} [m]
	43					
Minimum	1.0	0.059	0.059	1.0	0.059	0.059
Maximum	7.6	0.122	0.677	9.2	0.301	1.723
Mean	2.3	0.072	0.164	1.2	0.079	0.097

windows of 5-m or larger. In agreement with the moving window result from the Waikoloa dataset, it is suggested that a moving window with the smallest possible size should be considered. However, it must be large enough to ensure a sufficient number of points within the window to estimate terrain roughness (a minimum of 8 points/samples is adopted in this study following Milan et al. (2011)). Additionally, this may also be dependent on the interpolation method that is used, because some methods such as inverse distance weighting use more cloud points rather than just the three nearest points, which is the case for TIN interpolation. Therefore, trials should also be conducted to choose the best window size (\mathbb{R}^2 was used as the selection criteria in this study but other criteria, e.g., correlation coefficient, can also be tested) for the interpolation method used.

As previously presented, a relationship between zero-roughness and nonzero-roughness uncertainties is needed. Therefore, the relative standard deviation of interpolation error is estimated by dividing the standard deviation of interpolation error by the first value, i.e., that at 0 $\rm m^3/pt$, with the results shown in Fig. 12. Equation (8) is then used to

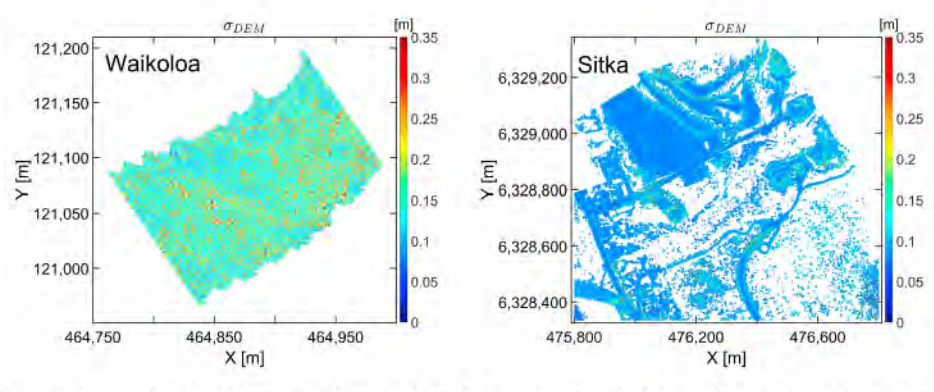
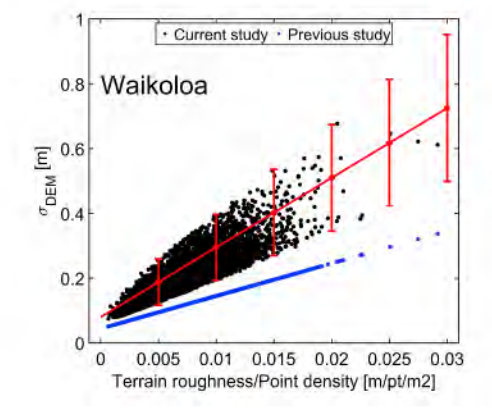


Fig. 13. Grid point uncertainty by scaled GLOPOV propagated uncertainty: (left) Waikoloa and (right) Sitka. Gaps in Sitka are caused by dense vegetation.



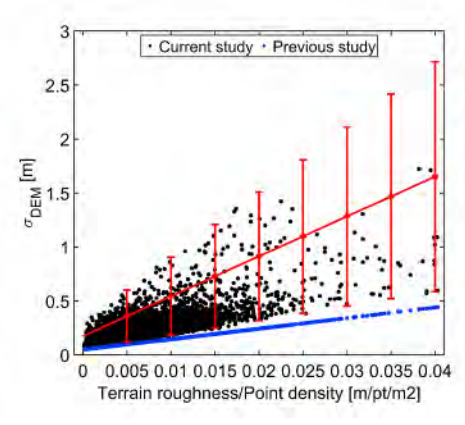


Fig. 14. Comparison of resultant uncertainty between current and previous studies: (Left) Waikoloa and (right) Sitka. Blue dots indicate the uncertainty estimated by applying the approach presented in Heritage et al. (2009) and Milan et al. (2011). Black dots indicate the results computed by the workflow proposed in this study with the variation about a linear trend indicated by red vertical bars. (For interpretation of the references to colour in this figure legend, the reader is referred to the Web version of this article.)

estimate the slope/y-intercept fraction (m) of 226.8411 (Waikoloa) and 203.0414 (Sitka) with coefficients of determination of 0.9822 (Waikoloa) and 0.9596 (Sitka).

The fraction $\frac{\sigma_{gp}}{\rho}$ is computed for all gridded points using a 1-m moving window, and then Equation (9) is used to estimate the scale factors. The resultant scale factors range between 1 (in flat areas) and 7.6 (Waikoloa) and 9.2 (Sitka) (in high roughness areas), with mean values of 2.3 (Waikoloa) and 1.2 (Sitka) (see Table 3). The final gridded DEM uncertainty (σ_{DEM}) is then estimated using Equation (10) with propagated gridded uncertainty and scale factors; the results are shown in Fig. 13 with their statistics given in Table 3.

The estimated uncertainty based on the proposed workflow in this study was then compared with that computed using the approach presented in Heritage et al. (2009) and Milan et al. (2011), with the results shown in Fig. 14. With the previous approach, the linear relationships between terrain roughness/point density and standard deviation of interpolation error as in Fig. 8 (right) are used to estimate gridded uncertainty by applying the estimated $\frac{\sigma_{tr}}{a}$. This indicates that only terrain roughness and point density are considered; as a result, the estimated gridded DEM uncertainty shows a linear behavior (see blue dots in Fig. 14). By contrast, in the current study, we have shown that, together with terrain roughness and point density, the estimated uncertainty of a gridded DEM is also dependent on the horizontal and vertical uncertainties of the cloud points, the inclination of the TIN triangles, and the locations of the gridded points relative to the TIN triangle vertices (see Bui et al. (2022) for more details); as a result, the uncertainty estimated herein shows variation about a linear trend. These varied ranges are indicated by the red vertical bars in Fig. 14 that are also changed according to the increase in terrain roughness/point density.

5. Conclusions

A realistic uncertainty propagation is crucial for airborne lidar so that the uncertainty of derived DEMs and derivative products, e.g., snow volume measured from change detection, can be accurately quantified. This paper proposed an end-to-end approach to quantify the uncertainty of gridded DEMs that are derived by interpolation from lidar-based point clouds using TIN interpolation.

The proposed approach can be utilized to quantify gridded DEM uncertainty without requiring independently validated data measured from a method other than the lidar data itself. In addition, both the horizontal and vertical point cloud uncertainties are dealt with simultaneously in the propagated and gridded uncertainty. This is important because the influence of horizontal uncertainty has been shown to be significant in steep terrain (i.e., surfaces with high slope angles) and cannot be neglected; consideration of only cloud point vertical uncertainty significantly underestimates propagated gridded point uncertainty.

The proposed approach has been applied to two airborne lidar datasets at Waikoloa, Hawaii and Sitka, Alaska to derive gridded DEM uncertainties by TIN interpolation. The candidate interpolation model tested in this study is TIN, but the proposed workflow can be easily extended to other models, such as nearest neighbor, IDW, linear or high-order polynomials. The uncertainties derived from this study are useful not only to show the confidence level of the derived DEM but also for uncertainty assessment in derivative products such as change maps or volumetric computations.

Declaration of competing interest

The authors declare that they have no known competing financial interests or personal relationships that could have appeared to influence the work reported in this paper.

Acknowledgement

Funding for this research was partially provided by grants from the National Geospatial-Intelligence Agency (HM047622-1-0003), the National Science Foundation (# 1830734), and the U.S. Army Corps of Engineers Cold Regions Research and Engineering Laboratory (USACE-CRREL). The data used in this study were collected and processed by the USACE-CRREL with assistance from the National Center for Airborne Laser Mapping. Nima Ekhtari is thanked for his assistance in the ground filtering applied to the Sitka dataset.

References

- Abd Aziz, S., Steward, B.L., Tang, L., Karkee, M., 2009. Utilizing repeated GPS surveys from field operations for development of agricultural field DEMs. Transactions of the ASABE 52 (4), 1057–1067.
- Aguilar, F.J., Mills, J.P., Delgado, J., Aguilar, M.A., Negreiros, J.G., Pérez, J.L., 2010. Modelling vertical error in LiDAR-derived digital elevation models. ISPRS J. Photogrammetry Remote Sens. 65 (1), 103–110. https://doi.org/10.1016/j.isprsjprs.2009.09.003.
- Agüera-Vega, F., Agüera-Puntas, M., Martínez-Carricondo, P., Mancini, F., Carvajal, F., 2020. Effects of point cloud density, interpolation method and grid size on derived Digital Terrain Model accuracy at micro topography level. Int. J. Rem. Sens. 41 (21), 8281–8299. https://doi.org/10.1080/01431161.2020.1771788.
- Brasington, J., Langham, J., Rumsby, B.T., 2003. Methodological sensitivity of morphometric estimates of coarse fluvial sediment transport. Geomorphology 53 (3-4), 299-316. https://doi.org/10.1016/S0169-555X(02)00320-3.
- Brasington, J., Rumsby, B.T., Mcvey, R.A., 2000. Monitoring and modelling morphological change in a braided gravel-bed river using high resolution GPS-based survey. Earth Surf. Process. Landforms 25 (9), 973–990. https://doi.org/10.1002/ 1096-9837(200008)25:9¡973::AID-ESP111¿3.0.CO;2-Y.
- Bui, L.K., Glennie, C.L., Hartzell, P.J., 2022. Rigorous propagation of LiDAR point cloud uncertainties to spatially regular grids by a TIN linear interpolation. Geosci. Rem. Sens. Lett. IEEE 19, 7003105. https://doi.org/10.1109/LGRS.2021.3134587.
- Carlisle, B.H., 2005. Modelling the spatial distribution of DEM error. Trans. GIS 9 (4), 521–540. https://doi.org/10.1111/j.1467-9671.2005.00233.x.
- DMA. Department of defense world geodetic system 1984 technical report, Part II: Parameters, formulas, and graphics for the practical application of WGS 84. https://earth-info.nga.mil/GandG/publications/tr8350.2/TR8350.2-b/DMA%20T PR350.pdf
- DMA. Department of Defense World Geodetic System 1984: Its definition and relationships with local geodetic systems. https://apps.dtic.mil/dtic/tr/fulltext/u2/a280358.pdf.
- Fan, L., Smethurst, J., Atkinson, P., Powrie, W., 2014. Propagation of vertical and horizontal source data errors into a TIN with linear interpolation. Int. J. Geogr. Inf. Sci. 28 (7), 1378–1400. https://doi.org/10.1080/13658816.2014.889299.
- Fuller, I.C., Large, A.R.G., Milan, D.J., 2003. Quantifying channel development and sediment transfer following chute cutoff in a wandering gravel-bed river. Geomorphology 54 (3-4), 307-323. https://doi.org/10.1016/S0169-555X(02)
- Ghilani, C.D., Wolf, P.R., 2010. Adjustment Computations: Spatial Data Analysis, fifth ed. John Wiley & Sons, Inc. https://doi.org/10.1002/9780470586266.
- Glennie, C.L., 2007. Rigorous 3D error analysis of kinematic scanning LIDAR systems. J. Appl. Geodes. 1 (3), 147–157. https://doi.org/10.1515/jag.2007.017.
- Glennie, C.L., Carter, W.E., Shrestha, R.L., Dietrich, W.E., 2013. Geodetic imaging with airborne LiDAR: the Earth's surface revealed. Rep. Prog. Phys. 76 (8) https://doi. org/10.1088/0034-4885/76/8/086801.
- Hartzell, P.J., Gadomski, P.J., Glennie, C.L., Finnegan, D.C., Deems, J.S., 2015. Rigorous error propagation for terrestrial laser scanning with application to snow volume uncertainty. J. Glaciol. 61 (230), 1147–1158. https://doi.org/10.3189/ 2015JoG15J031.
- Heritage, G.L., Milan, D.J., Large, A.R.G., Fuller, I.C., 2009. Influence of survey strategy and interpolation model on DEM quality. Geomorphology 112 (3-4), 334-344. https://doi.org/10.1016/j.geomorph.2009.06.024.
- Hodgson, M.E., Bresnahan, P., 2004. Accuracy of airborne lidar-derived elevation: empirical assessment and error budget. Photogramm. Eng. Rem. Sens. 70 (3), 331–339. https://doi.org/10.14358/PERS.70.3.331.
- Hu, P., Liu, X., Hu, H., 2009. Accuracy assessment of digital elevation models based on approximation theory. Photogramm. Eng. Rem. Sens. 75 (1), 49–56. https://doi.org/ 10.14358/PERS.75.1.49.
- Kidner, D.B., 2003. Higher-order interpolation of regular grid digital elevation models. Int. J. Rem. Sens. 24 (14), 2981–2987. https://doi.org/10.1080/ 0143116031000086835.
- Kyriakidis, P.C., Goodchild, M.F., 2006. On the prediction error variance of three common spatial interpolation schemes. Int. J. Geogr. Inf. Sci. 20 (8), 823–855. https://doi.org/10.1080/13658810600711279.
- Liu, X., 2008. Airborne LiDAR for DEM generation: some critical issues. Prog. Phys. Geogr. 32 (1), 31–49. https://doi.org/10.1177/0309133308089496.
- Liu, X., Zhang, Z., Peterson, J., Chandra, S., 2007. The effect of LiDAR data density on DEM accuracy. In: MODSIM 2007 - International Congress on Modelling and Simulation - Land, Water and Environmental Management: Integrated Systems for Sustainability, Proceedings, pp. 1363–1369.

- Milan, D.J., Heritage, G.L., Large, A.R.G., Fuller, I.C., 2011. Filtering spatial error from DEMs: implications for morphological change estimation. Geomorphology 125 (1), 160-171. https://doi.org/10.1016/j.geomorph.2010.09.012.
- Ouédraogo, M.M., Degré, A., Debouche, C., Lisein, J., 2014. The evaluation of unmanned aerial system-based photogrammetry and terrestrial laser scanning to generate DEMs of agricultural watersheds. Geomorphology 214, 339–355. https://doi.org/10.1016/j.geomorph.2014.02.016.
- Rabus, B., Eineder, M., Roth, A., Bamler, R., 2003. The shuttle radar topography mission - a new class of digital elevation models acquired by spaceborne radar [Journal Article]. ISPRS J. Photogrammetry Remote Sens. 57 (4), 241–262. https://doi.org/ 10.1016/S0924-2716(02)00124-7.
- Rees, W.G., 2000. The accuracy of Digital Elevation Models interpolated to higher resolutions. Int. J. Rem. Sens. 21 (1), 7-20. https://doi.org/10.1080/ 014311600210957.
- Schaer, P., Skaloud, J., Landtwing, S., Legat, K., 2007. Accuracy estimation for laser point cloud including scanning geometry. In: 5th International Symposium on Mobile Mapping Symposium (padova).
- Shi, W.Z., Li, Q.Q., Zhu, C.Q., 2005. Estimating the propagation error of DEM from higher-order interpolation algorithms. Int. J. Rem. Sens. 26 (14), 3069-3084. https://doi.org/10.1080/01431160500057905.
- Skaloud, J., Schaer, P., 2012. Automated assessment of digital terrain models derived from airborne laser scanning. Photogramm. Fernerkund. GeoInf. 2, 105–114. https://doi.org/10.1127/1432-8364/2012/0105.

- Smith, M.P., Zhu, A.X., Burt, J.E., Stiles, C., 2006. The effects of DEM resolution and neighborhood size on digital soil survey. Geoderma 137 (1-2), 58-69. https://doi. org/10.1016/j.geoderma.2006.07.002.
- Spaete, L.P., Glenn, N.F., Derryberry, D.R., Sankey, T.T., Mitchell, J.J., Hardegree, S.P., 2011. Vegetation and slope effects on accuracy of a LiDAR-derivedDEMin the sagebrush steppe. Remote Sens. Lett. 2 (4), 317–326. https://doi.org/10.1080/ 01431161.2010.515267.
- Su, J., Bork, E., 2006. Influence of vegetation, slope, and lidar sampling angle on DEM accuracy. Photogramm. Eng. Rem. Sens. 72 (11), 1265–1274. https://doi.org/ 10.14358/PERS.72.11.1265.
- Wechsler, S.F., Kroll, C.N., 2006. Quantifying DEM uncertainty and its effect on topographic parameters. Photogramm. Eng. Rem. Sens. 72 (9), 1081–1090. https:// doi.org/10.14358/PERS.72.9.1081.
- Wheaton, J.M., Brasington, J., Darby, S.E., Sear, D.A., 2010. Accounting for uncertainty in DEMs from repeat topographic surveys: improved sediment budgets. Earth Surf. Process. Landforms 35 (2), 136-156. https://doi.org/10.1002/esp.1886.
- Zhu, C., Shi, W., Li, Q., Wang, G., Cheung, T.C.K., Dai, E., Shea, G.Y.K., 2005. Estimation of average DEM accuracy under linear interpolation considering random error at the nodes of TIN model. Int. J. Rem. Sens. 26 (24), 5509–5523. https://doi.org/10.1080/10245330500169029.